Initial shape reconstruction of a volcanic island as a tool for quantifying long-term coastal erosion: the case of Corvo Island (Azores)

Rémi Bossis[1], Vincent Regard[1], Sébastien Carretier[1]

5   [1]GET, University of Toulouse, CNRS, IRD, UPS, Toulouse, 31400, France

Correspondence to: Rémi Bossis (remi.bossis@get.omp.eu)

Abstract. Long-term coastal erosion is not yet well studied given that it is difficult to quantify. The quantification of long-term coastal erosion requires a proper reconstruction of the coast's initial geometry. It is also important to determine the timing of the start-up. Volcanic islands are good candidates fulfilling these two conditions: their initial shape is roughly

10   conical and the age of the lavas that generated this geometry is easily measured. We have developed a method to reconstruct the initial shape of simple volcanic edifices from aerial and submarine topographic data. The reconstructed initial shape and associated uncertainties allow us to spatially quantify the coastal erosion since the building of the island. This method is applied to Corvo Island in the Azores archipelago. We calculated the initial radius and peak elevation of the island to be approximately 3.8 km and 1 km, respectively. We calculated that, due to coastal erosion, the island has lost a volume of 6.5

15   ± 2.7 km³ corresponding to a reduction of roughly 80% of its surface area since it was first built. Taking the large uncertainty in the age of the topmost lava flows (90 to 770 ka) into account, our reconstruction yields a conservative range of long-term coastal erosion rates between 7 and 370 mm/yr. These values are consistent with the orders of magnitude of short-term coastal erosion rates measured on similar lithologies. Lastly, we show a strong correlation between long-term coastal erosion and the spatial distribution of the waves. Specifically, we highlight a stronger erosion control by moderate and usual waves

20   than by storm waves. The next step will be to apply this method to other volcanic islands in order to: (i) strengthen and consolidate the method, and (ii) verify the correlations observed in the present study.

1 Introduction

Rocky coast erosion is mainly driven by wave action at the feet of coastal cliffs (Sunamura, 1992; e.g. Anderson et al., 1999; Trenhaile, 2000). The number of studies performed to quantify rocky coast erosion has increased dramatically since the

25   1990s (Prémaillon et al., 2018), following the massive anthropization of the coast in the second half of the 20th century (Robert, 2019). Coastal erosion has primarily been studied and quantified through the direct comparison of the cliff top position over time, mainly from aerial photographs, lidar or UAV derived photogrammetry, on a monthly to a multi-decadal scale (Bird, 2011; Moses and Robinson, 2011; Dewez et al., 2013; Rosser et al., 2013; Letortu et al., 2015; Costa et al., 2019; Prémaillon et al., 2021; Young et al., 2021). Recent research on this phenomenon has focused on the coastline of developed

30   countries, mainly France (e.g. Dewez et al., 2013; Letortu et al., 2015; Roulland et al., 2019; Duguet et al., 2021; Prémaillon et al., 2021), the UK (Dornbusch et al., 2008; Lim et al., 2010; Rosser et al., 2013; e.g. Buchanan et al., 2020), Portugal (Dias and Neal, 1992; e.g. Catalão et al., 2002; Marques et al., 2013), the west coast of the USA (e.g. Anderson et al., 1999; Benumof et al., 2000; Hapke et al., 2009; Young et al., 2021), and New Zealand (e.g. Gibb, 1978; Grant, 1981; Kennedy and Dickson, 2007; Micallef et al., 2021).

35   Coastal erosion has therefore been studied almost exclusively on a short-term timescale of less than one century, and under a temperate climate (Prémaillon et al., 2018; Young and Carilli, 2019). Over the long term, i.e. over several thousand to millions of years, it is more complicated to quantify coastal erosion because geomorphic markers may have been eroded and are poorly dated. However, more emphasis should be placed on long-term coastal erosion so as to place short-term measurements within the context of long-term trends. Given that coastal erosion is a discontinuous phenomenon over time,

40   short-term measurements may omit the existence of catastrophic events, such as cliff collapse, which occur only very rarely over the short term (Lim et al., 2010; e.g. Dewez et al., 2013; Rohmer and Dewez, 2013). Long-term measurements take these events into account and therefore, if they are obtained they could, for example, be used to quantify a delay in the short-term versus long-term cliff retreat. This could be an indicator of a nearby catastrophic event, and thus of a potential hazard. On the other hand, the overall flux of material from the continent to the ocean is generally reduced to the input of sediment

45   from rivers and is estimated to be approximately 19 Gt/yr (Milliman and Farnsworth, 2013). Coastal erosion is another flux of material from the continent to the ocean, but because it is difficult to quantify, this means that its contribution is generally overlooked (Regard et al., 2022). Regional studies (Rachold et al., 2000; Landemaine, 2016) have shown that the contribution of coastal erosion in this flux could be very large, up to twice that of fluvial discharge in the case of the Laptev Sea coastline (Rachold et al., 2000). For Europe, Regard et al. (2022) re-evaluated the sediment generated by rocky coast

50   erosion to one third of the fluvial contribution, which is much higher than previously estimated. In the long term, coastal erosion may thus significantly affect the surface of continents and global geochemical cycles. Lastly, the study of short-term coastal erosion has allowed to show that rock strength controls it to the first order (Prémaillon et al., 2018). Yet, it is unclear if the same holds true over the long-term, when other factors such as eustasy become significant (Trenhaile, 2001; Anderson and Anderson, 2010; Quartau et al., 2018). As a result, there is a gap in knowledge with regards to coastal erosion over long-

55   term scales.

The difficulty in quantifying long-term coastal erosion comes from the lack of direct measurements of cliff retreat at that timescale. Cosmogenic nuclides have been applied along cross-shore profiles in order to quantify the mean rate of cliff retreat (e.g. Hurst et al., 2016; Raimbault et al., 2018; Regard et al., 2022). These approaches are promising but give a local millennial mean retreat rate and require a long analytical process. A complementary approach consists of evaluating the

60   topography difference from the reconstructed topography at different epochs. This measure of erosion rate requires the quantification of the eroded volume and the time over which the erosion occurred. The ideal configuration consists of a monogenic massif whose age and initial geometry are known. This ideal configuration is rare (Bird, 2011), but can be, however, found on volcanic islands. The coastlines of oceanic volcanic islands have the advantage of having been

established at a well-defined time, during the emergence of a volcano. Conversely, its end is relatively predictable, with the
65   disappearance of the island under subsidence or erosion (Ramalho et al., 2013).

Furthermore, if the island consists of a simple, radially symmetrical volcanic edifice, it can be assumed that the slope of its
flanks is regular or evolves regularly from the top of the edifice to the shoreline (Karátson et al., 2010). Therefore, the shape
of a radially symmetrical volcanic island can be fitted by the revolution of a function curve around the center of the edifice
(Lahitte et al., 2012; e.g. Favalli et al., 2014; Karátson et al., 2016).

70   The growth of a volcanic island is mainly due to the successive superposition of lava flows emitted during eruptions
(Peterson and Moore, 1987; e.g. DePaolo and Stolper, 1996). This volcanic activity is a discontinuous phenomenon in time
and on the surface of the island (e.g. Lipman, 1995; Sherrod et al., 2006). Therefore, the surface of a volcanic island cannot
be perfectly synchronous, and the maximum extension cannot have the same age all around the island. However, large
variations in volcanic activity around an island over the long term would lead to a change in the global shape of the island
75   and a weakening of the radial symmetry of the volcanic edifice (e.g. Germa et al., 2010; Quartau et al., 2010, 2014). Thus,
volcanic island radial symmetry indicates that its volcanic activity has remained homogeneously distributed around the
edifice and that the last flows constituting the surface of the island have close ages on the scale of the island's lifetime.
Therefore, unless the age of the different flows constituting the initial shoreline of the island is precisely known, coastal
erosion likely began at about the same time all around the island.

80   In this study, "initial" shape refers to the theorical surface of the volcanic island at the moment of its maximum extension
during its history. In terms of timing in the history of the island, this maximum extension corresponds to the transition from
the growth phase, to the degradation phase of the edifice. During the growth phase, volcanic progradation, with the
formation of lava deltas, extends the shoreline (Ramalho et al., 2013) and dominates the erosive processes, whereas during
the degradation phase, erosive processes become predominant (Ferrer-Valero and Hernández-Calvento, 2020). We consider
85   that this transition marks when the coastal erosion began. It is hard to know whether this transition is gradual or punctual, as
well as to date this moment. This moment likely follows the setting of the flows constituting the top of the sea-cliffs, and
thus the age of these flows indicates the age of the "initial" shape.

In the case of volcanic islands, it is therefore possible to simultaneously reconstruct the initial shape of the coastline by
surface fitting and to estimate the age of the start of the coastal erosion. This reconstruction may be achieved using
90   topographic data (Favalli et al., 2014). Consequently, it is possible to calculate the average coastal erosion rate over the long-
term (Menard, 1983; Quartau et al., 2010).

Volcanic islands are widespread across the world. An automatic quantification of the erosion rates would make it possible to
study the influence of factors such as climate or geodynamics on these erosion rates and hence to determine their relative
importance with regards to long-term erosion rates. A first step forward, described in the present work, consists in the
95   development of a tool to reconstruct the initial aerial and submarine volcano island relief.

2 Background and hypotheses

Hildenbrand et al. (2008), Germa et al. (2010, 2015), Lahitte et al. (2012), Salvany et al. (2012), Lavigne et al. (2013), Torrecillas et al. (2013), Ricci et al. (2015a, 2015b), and Karátson et al. (2016) have proposed various methods for reconstructing the initial onshore shape of volcanic islands. These methods are based on the analysis of the onshore

100 topography and spatial distribution of geological units on a volcanic island. These methods consist in determining which geological units and which part of the current topography of a volcanic island are representative of its maximum extension and initial shape. Then, using topographic data, the initial edifice topography can be reconstructed either by kriging interpolation (e.g. Hildenbrand et al., 2008; Germa et al., 2010) or by using a synthetic solid of revolution for the 3D geometry if the island is radially symmetric (e.g. Karátson et al., 2016).

105 The aim of these methods is to quantify the total aerial erosion of each studied volcano in order to establish the geomorphological evolution of these volcanoes. When applied to volcanic islands, these methods reconstruct the edifice down to the intersection with the sea level, and can be used to estimate the maximum island extension. However, volcanic island edifices are not limited to their aerial part. As a result, the methods that reconstruct the volcano morphology ignore the submarine geomorphology. Yet, the submarine realm of volcanoes offers other constraints to better reconstruct the initial

110 edifice geometry and to quantify coastal erosion, as seen in the next section.

Coastal erosion results in the formation of an erosional shelf below sea level and a coastal cliff above sea level in the nearshore zone (Trenhaile and Bryne, 1986; Sunamura, 1992; Anderson and Anderson, 2010; Ramalho et al., 2013). The junction between the shelf and the cliff corresponds to the foot of the coastal cliff; this will be referred to as the shoreline angle (SLA) (Fig. 1). The vertical position of the SLA does not depart from the current mean sea level by more than a few

115 meters (Wright, 1970; Trenhaile, 1972; Anderson and Anderson, 2010). In the water column, wave energy decreases rapidly with depth. The dispersion of this energy can significantly erode the bedrock until about 10 m below sea level, a depth that corresponds to the downward wave action limit (Quartau et al., 2010). The maximum of erosion takes place where the water depth is similar to the mean wave height (Trenhaile, 2000, 2001). The erosional shelf therefore has a theorical depth ranging from around 0 m at the coast to about 10 m at the shelf edge (Fig. 1). At the coast, the waves weaken the cliff base through a

120 variety of phenomena, leading to a stochastic gravitational collapse over time. The real cliff collapse process is beyond the scope of this study, we assume that cliff collapse occurs frequently at the millennial timescale. Thus, the succession of gravitational collapses results in cliff retreat, which may be related to wave energy (Trenhaile, 2001; Anderson and Anderson, 2010; Ramalho et al., 2013).
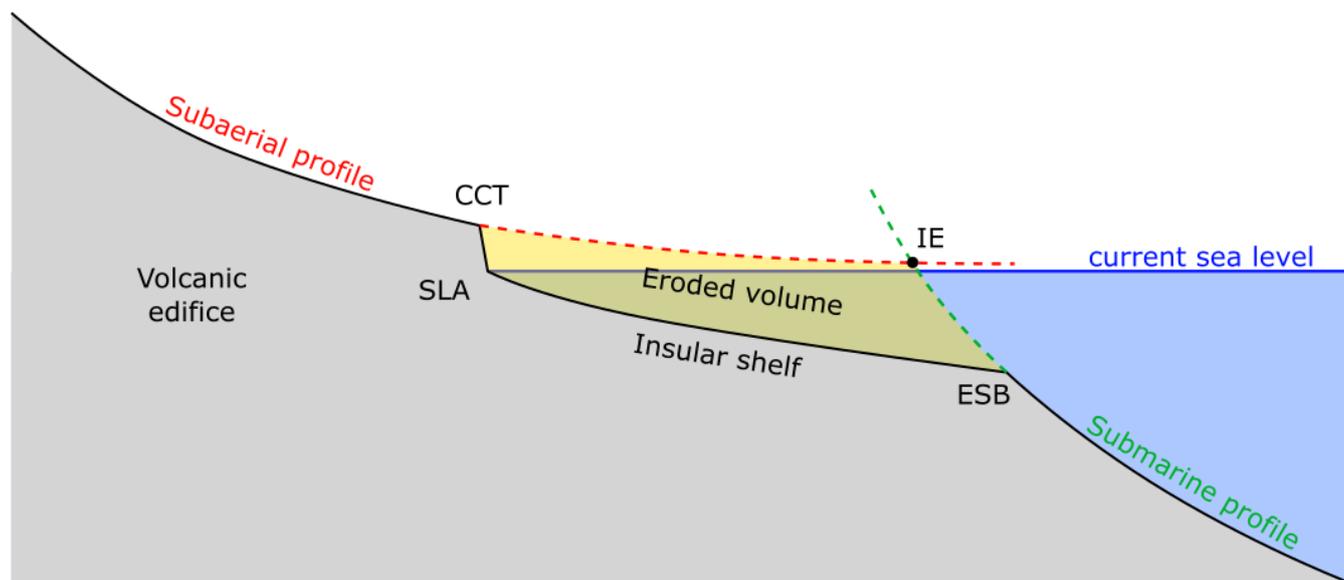
Figure 1: Schematic representation of a radial topographic profile of a volcanic island. The initial aerial and submarine profiles are demarcated with dashed lines. CCT: Coastal Cliff Top. SLA: Shoreline Angle. ESB: Erosional Shelf Break. IE: Initial Extension.

In the case of volcanic islands, the erosional shelf that generally surrounds the aerial part of the volcanic edifice is called an insular shelf (e.g. Quartau et al., 2010; Ramalho et al., 2013). The inner bound of this shelf is the base of the coastal cliff and its outer bound is the shelf break. This latter is characterized by a rapid increase in the slope from a few degrees on the shelf to a greater slope seaward; the threshold is sometimes fixed to 15 degrees (Quartau et al., 2010). The depth of the shelf break theoretically corresponds to the limit of wave action during the lowest eustatic level the island has experienced (Quartau et al., 2010; Ramalho et al., 2013). If the island is older than the last glacial maximum and its vertical displacement is negligible, the depth of the shelf break is theoretically 130 m, i.e. LGM level (120 m) + wave action limit (10 m) (Shepard, 1973; Trenhaile, 2001; Quartau et al., 2010). If the shelf edge has been covered by sediments or by volcanic progradation, the apparent depth of the shelf break is reduced; in this case, the shelf break is called a depositional shelf break (DSB) (Quartau et al., 2010). On the contrary, if it has not been covered by any material, it is called an erosional shelf break (ESB) (Quartau et al., 2010).

In summary, the range of coastal erosion is spatially limited by the ESB on its ocean side and by the cliff up to its top (Coastal Cliff Top or CCT) on its land side (Fig. 1). It is possible to consider that the aerial part of the volcanic edifice above the CCT is only subject to fluvial erosion, whereas the submarine part of the edifice below the ESB (Fig. 1) is not subject to any erosive process except for gravitational collapses at the shelf edge which may form an embayment (Ramalho et al., 2013; Chang et al., 2021).

For edifices with a radial symmetry, the topography can be subdivided into one aerial and one submarine radial profile (Mitchell et al., 2002). Following the models of Peterson and Moore (1987), DePaolo and Stopler (1996) and Ramalho et al. (2013), we can estimate the volcano aspect before coastal erosion via two extended radial profiles. The first one is aerial; it

runs from the volcano center to the CCT. The second profile is submarine, below the ESB (Fig. 1). These two profiles intersect at a point called the initial extension (IE) that corresponds to the theorical original boundary between the aerial and submarine parts of the edifice. The IE is the reference used to calculate the coastal erosion.

150   Theoretically, the IE must be located near the sea level at the time of volcanic island-building. Thus, the IE could also serve as a proxy for estimating the total vertical motion experienced by the island since its formation. If the IE is above sea level, the island may have experienced a total uplift relative to the sea level corresponding to the elevation of the IE. Conversely, an IE below sea level indicates that the island underwent significant subsidence. This vertical motion estimation is relative to the sea level; consequently, it is highly dependent on the eustatic level at the time of volcanic activity. The sea level at this

155   time can be estimated through sea level curves (Shackleton, 2000; Waelbroeck et al., 2002; Bintanja and van de Wal, 2008; Rohling et al., 2009; Spratt and Lisiecki, 2016), but nevertheless requires that the volcano age is well known, which is quite challenging, as seen in the following.

Coastal erosion is traditionally measured by a value of total horizontal retreat (in m); it can be derived as a rate per unit of time (m/year). However, as presented, coastal erosion not only causes cliff retreat (horizontal) but also occurs vertically,

160   from the ESB to the CCT. Therefore, the calculation of a horizontal retreat rate requires an accurate definition of the most relevant geomorphological markers. For example, if the coastal cliff top (CCT) is used as a reference, then the most relevant estimate of the horizontal coastal retreat distance is the IE-CCT distance. If the width of the insular shelf is taken as the reference, as in Menard (1983, 1986) and Quartau et al. (2010, 2014), then the most relevant measure is the ESB-SLA (shoreline angle) distance. Alternatively, we could consider the retreat of the cliff base, i.e. the SLA, and then the SLA-IE

165   distance would be the most relevant. Lastly, if we want to include the entire area affected by coastal erosion, then the ESB-CCT distance would be relevant.

Moreover, as shown in the model of Ramalho et al. (2013, Fig. 8), coastal erosion will not affect the same area of the coast depending on the eustatic level (Huppert et al., 2020). For example, during a sea level highstand, i.e. during an interglacial period, coastal erosion occurs mostly horizontally via coastal cliff retreat, whereas during sea level fall or lowstand, i.e.

170   during a glacial period, coastal erosion affects only the erosional shelf, in such a way that its surface appears to move downward, which is sometimes called downwearing. In the latter case, the ESB not only moves deeper but also farther from the shoreline, increasing the width of the insular shelf, as well as the apparent amount of coastal erosion.

These different phases challenge the significance of a horizontal measurement of long-term coastal erosion. Along a radial profile, it might be more relevant to calculate an eroded volume normalized by the coastline length (m^3/m, sometimes

175   reduced to m^2), which corresponds to the area between the four geomorphological markers proposed here, i.e. CCT, SLA, ESB and IE (Fig. 1). However, in order to compare long-term coastal erosion metrics with traditionally calculated short-term metrics, it seems necessary to use the position of the coastal cliff top as a benchmark, so that the IE-CCT distance quantifies the erosion.

In conclusion, the approach of previous works, which only consider the aerial part of volcanic edifices, seems limited in

180   terms of reconstructing the initial geometry of the coastline because it omits the geomorphological specificities related to

long-term coastal erosion. We therefore propose here a new method based on the analysis of aerial and submarine topographic data of volcanic islands. This method considers all of these specificities and allows us to reconstruct a more realistic initial shape of the coastline.

3 Method

3.1 Workflow and preliminary comment

This method aims to quantify the volume of material removed by coastal erosion on volcanic islands. The method steps are the following (Fig. 1):

- We assume a radial symmetry of the island (or part of it) and determine its center.
- We reconstruct the pre-erosion aerial topography of the island along stacked radial profiles.
- We reconstruct the submarine topography of the island along stacked radial profiles.
- The intersection between the aerial and submarine profiles allows us to calculate an eroded volume and its uncertainty according to the uncertainties on reconstructed aerial and submarine topographies.

Compared to a simple measurement of shelf width, which quantifies the total retreat of coastal cliffs (e.g. Quartau et al., 2010), this method is used not only to calculate an eroded volume and its uncertainty, but also to provide evidence that portions of the shelf have possibly been lost due to gravity collapses.

Because it is based on topography reconstruction, this method relies on a long-term integrative view of coastal erosion and does not aim to represent the complex geomorphological evolution of coastal cliffs and insular shelves related to the interplay between the processes involved (Ramalho et al., 2013). In order to provide a simple method that can be easily applied to a large number of study sites, the method is based on simple and intentionally reductionist working hypotheses, and at the same time on a careful estimation of the uncertainty on eroded volumes that would be less constrained by considering only the aerial topography alone. Some of the hypotheses can be adapted according to the available data. For example, the hypothesis of complete radial symmetry of the volcanic edifice adopted to treat the following illustrative case study is not mandatory for our approach. For other islands, radial symmetry can be assumed for only a portion of the island. This flexibility allows to obtain exploitable and directly comparable coastal erosion values between the different sites where the method is applied.

We illustrate this method on a simple case. We first detail the different steps of the method, then we describe the case study of Corvo Island.

3.2 Choice of island

The method proposed here is based on the hypothesis of a simple geometry of volcanic edifices. This method is therefore preferentially applied to volcanic islands composed of a single central edifice that is roughly conical in shape with a

dominant radial symmetry, similar to many stratovolcanoes (Karátson et al., 2010). Alternatively, it can be applied to a portion of an island that meets these criteria. Suitable islands for this method might be mainly young volcanic islands with a simple and known volcanic history. Another selection criterion is the availability of high-resolution aerial and submarine topographic data. These two data sets are necessary to reconstruct the initial aerial and submarine profiles of the island and

215 to determine the maximum extension of the island. For the aerial part, the 30 m resolution SRTM1 and ASTER global databases are sufficient to capture the geometry of volcanic islands with a diameter larger than 1 km. On the contrary, global bathymetric databases, such as GEBCO, only offer a horizontal resolution of approximately 500 m, which is insufficient to account for the submarine geometry of the edifice and to clearly identify an insular shelf. High resolution bathymetric data (a horizontal resolution of at least 50 m) around the island are therefore necessary to clearly identify the boundary between the

220 insular shelf and the non-eroded submarine slopes of the volcanic edifice.

3.3 CCT and ESB mapping

Identifying the CCT is quite simple: it is generally a fairly marked break in slope on the edges of the island. It can be mapped on satellite imagery as well as on topographic data except, for example, when this break in slope is smoothed by strong aerial erosion. The CCT corresponds to the inflexion point where the slope starts to increase oceanward.

225 The ESB corresponds to a gentler break in slope than the cliff top; it instead corresponds to a smooth transition, tens to hundreds of meters wide, from a slope of a few degrees on the insular shelf to a slope of a few tens of degrees on the submarine slopes of the volcanic edifice. Following Quartau et al. (2010), we have chosen a slope threshold of 15° in order to map the ESB.

The mapping of the CCT and ESB results in two concentric polygons (Fig. 2). The area in between these polygons is

230 identified as being the area where coastal erosion takes place. The area outside this area is considered to have been little altered by erosion, and therefore it is still very close to the initial shape of the volcanic edifice: its aerial part, with the exception of the caldera, corresponds to the initial aerial volcano shape; its submarine, outside, part represents the initial submarine shape.
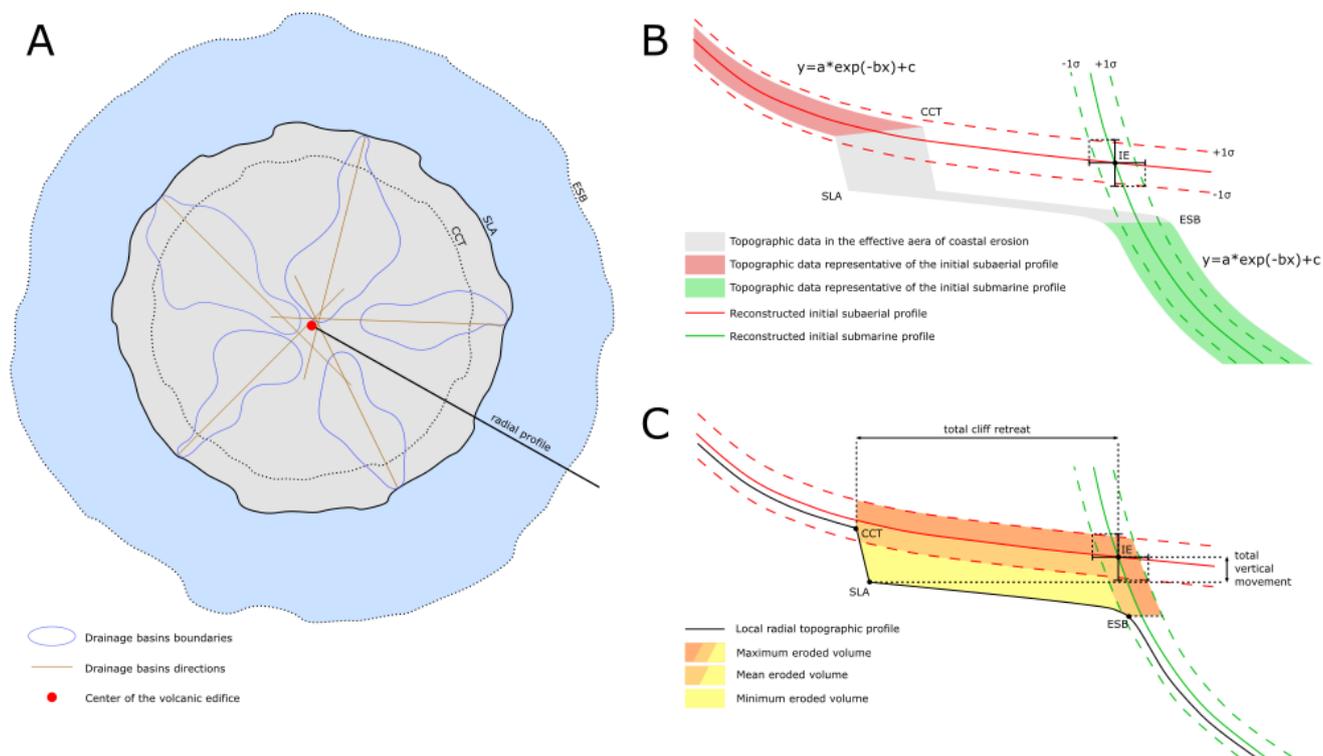
Figure 2: Topographic reconstruction method. A: Mapping of the CCT and ESB markers, and determination of the center of the edifice. Overhead view. B: Calculation of the radial aerial and submarine topographic profiles representative of the initial shape. C: Quantification of the cliff retreat, eroded volume and vertical movement.

3.4 Determination of the center of the volcanic edifice

In the following, it is necessary to determine the horizontal position of the center of symmetry of the volcanic edifice. Defining it is a prerequisite for defining the radial profiles. This point does not necessarily correspond to the center of the central crater. One solution is to calculate the barycenter of the concentric elevation contours, but this method is only applicable for very regular edifices that have experienced very little erosion (Karátson et al., 2010). The aim of the present work is to study various edifices, some of which have experienced significant, albeit variable, coastal erosion around the island. Instead, we have chosen a second method developed by Favalli et al. (2014) to determine the center of Mount Somma (Italy), a highly eroded edifice of which only the northwestern part of the slopes remain. This method determines the position of the center of the edifice as the center point of the radial drainage network (Fig. 2). The contours of the watershed are determined based on topographic data. The top of the watershed and its outlet are then extracted: the watershed direction is defined as the line connecting the two points. The directions of the different watersheds intersect in the summit area of the island. The center of the volcanic edifice is then defined as the barycenter of the intersection points of the watershed directions.

3.5 Radial distance-elevation profiles

Once the center of the edifice is determined, the distance of each point in the aerial and submarine topographic data to the center is calculated. This is use to represent the elevation of each data point as a function of its distance to the center (radial profile). It also allows to calculate two best-fit regression curves, one for the aerial points inside the CCT, and one for the submarine part outside the ESB (Fig. 2). Following the work of Karátson et al. (2010, 2016) and Favalli et al. (2014), we fit the data with a decreasing exponential because it is best suited for the type of volcano we are interested in, i.e. initially radially symmetric stratovolcanoes (Favalli et al., 2014; Karátson et al., 2016). The general form of this regression function is:

$$y = a\,e^{-bx} + c , \tag{1}$$

where y is the elevation, x is the distance to the center of the edifice, and a, b, and c are the parameters of the equation. The uncertainty is propagated by calculating the bounds of this regression at ±1σ, with $y + 1\sigma = y + \Delta y$ and $y - 1\sigma = y − \Delta y$. Δy is calculated by taking the total derivative of y according to a, b and c, leading to the following equation:

$$\Delta y = e^{-bx}\Delta a + x\,e^{-bx}\Delta b + \Delta c , \tag{2}$$

where Δa, Δb and Δc are the respective residual standard errors on the parameters a, b and c. The intersection of both the aerial and submarine exponential radial profiles estimates the position of the geomorphic marker IE. The intersections of the ±1σ bounds result in the estimation of both vertical and horizontal uncertainties in the position of the IE (error bars in Figure 2).

The calculated aerial exponential profile is close to, but probably below, the original surface of the island. Hillslope and fluvial erosion may have lowered the surface of the island during its history. Germa et al. (2010, 2015), Lahitte et al. (2012) and Ricci et al. (2015a, 2015b) solve this problem by only considering the hillcrest points in the calculation of the regression curve, which are a priori the least eroded points of the surface. Favalli et al. (2014) solve this problem by increasing the weight of the highest points during the regression. Meanwhile, Karátson et al. (2016) select the most representative surface points using morphometric indices and focusing on the planèzes to perform the regression. Here, we decided to keep all the points within the CCT polygon shape in GIS to perform the regression. This ensures that we keep a sufficient number of points for the regression. This simple method is the one that is the most widely applicable to as many volcanoes as possible, while local improvements can be carried out depending on the available geological information, without affecting the core of our method. In addition, this choice has the advantage of being as conservative as possible, i.e. not overestimating the calculated eroded volume.

3.6 Quantification of coastal erosion and vertical movement

The calculated radial profiles can be converted into a synthetic initial shape by creating a surface of revolution, i.e. rotating the profile around the radial axis of symmetry that is the center of the edifice (Lahitte et al., 2012; Favalli et al., 2014; Karátson et al., 2016). The total eroded volume of the island can be calculated by the difference between the calculated

initial topography and the current topography. The eroded volume related to coastal erosion corresponds to the part of this calculated volume contained in between the CCT and the ESB (Fig. 2). The uncertainty on the altitude of the profile (Δy) is

285 typically of the order of 10 to 100 m. The volume below the calculated -1σ profile is the minimum eroded volume, the volume below the calculated mean profile is the mean eroded volume, and the volume below the calculated +1σ profile is the maximum eroded volume (colors from yellow to salmon, respectively, in Fig. 2). The total cliff retreat is the distance between the IE and the local CCT position, and the horizontal error bar of the IE gives the uncertainty. Thus, it is possible to quantify a total eroded volume related to the coastal erosion. It is possible to further spatially quantify the degree to which

290 the calculated eroded volumes depend on the position at the edge of the island (with respect to the center of the island, denominated "sector" in the following). Moreover, the difference between the calculated IE elevation and the current sea level could be used to estimate the total subsidence or uplift, relative to the current sea level, that the island has experienced, with the uncertainty of the vertical error bar of the IE. Lastly, by relating the total cliff retreat to the age of maximum island extension it becomes possible to deduce the long-term integrated retreat rates.

295 4 Corvo Island settings and available data

4.1 Presentation of Corvo Island

The Azores are a volcanic archipelago located in the middle of the North Atlantic Ocean at the junction between the American, Eurasian and Nubian plates. The archipelago consists of nine main islands; two of them, Corvo and Flores, are on the American plate, and the others are on the wide border between the Eurasian and Nubian plates. These islands are quite

300 young (2 Ma to the present), modest in size (a few kilometers to tens of kilometers wide) and of modest elevation (a few hundred meters), with the exception of Pico Island, the elevation of which exceeds 2 km. The archipelago is characterized by a temperate oceanic climate that is rather humid and with mild temperatures. However, in this region, autumn and winter are marked by frequent storms, characterized by a strong wave regime from the west and northwest (Rusu and Guedes Soares, 2012). The Azores Islands are largely impacted by these storms, especially as the temperate climate prevents the

305 development of protective coral reefs (Quartau et al., 2012). The tidal range in the archipelago is less than 2 m (Ávila et al., 2005).

The modest elevation of these islands moderates the phenomenon of orographic precipitation (Ramalho et al., 2013) which makes the relics of their initial aerial volcanic morphology relatively well preserved from aerial erosion. This makes it possible to reconstruct their geological and morphological history (Quartau et al., 2014). In addition, the oceanic climate and

310 frequent storms expose the archipelago to strong coastal erosion, resulting in the formation of large coastal cliffs. These characteristics make the Azores a prime location for the study of coastal erosion and the evolution of coastal morphology on volcanic islands (Quartau et al., 2010, 2012, 2014, 2018; Ramalho et al., 2017; Melo et al., 2018; Ng et al., 2019).

Corvo is the smallest of the main islands and the northernmost island of the archipelago (Fig. 3). This small island measures approximately 5 km on its north-south axis and 3 km on its east-west axis. It is dominated by a volcanic edifice, Central

315 Volcano, which reaches 720 m in elevation and whose caldera measures approximately 2 km in diameter. This edifice, which gives its general shape to the island, was formed 0.43 ± 0.34 Ma ago and is composed of alkaline basalts (Dias, 2001; França et al., 2006). Another smaller and younger edifice, forming parasitic cones, has developed on the southern slope of the island, overlying the older volcanic morphology of the central volcano. Its last eruption occurred 80-100 ka ago (Dias, 2001; França et al., 2002, 2006). The island's coastline is almost exclusively made up of very high coastal cliffs, ranging

320 from 150-200 m high in the east to more than 600 m in the west, except in the south, where the coast consists of a lava delta from the youngest edifice and has been anthropized by the installation of coastal infrastructures and an airfield (França et al., 2002; Pacheco et al., 2013).
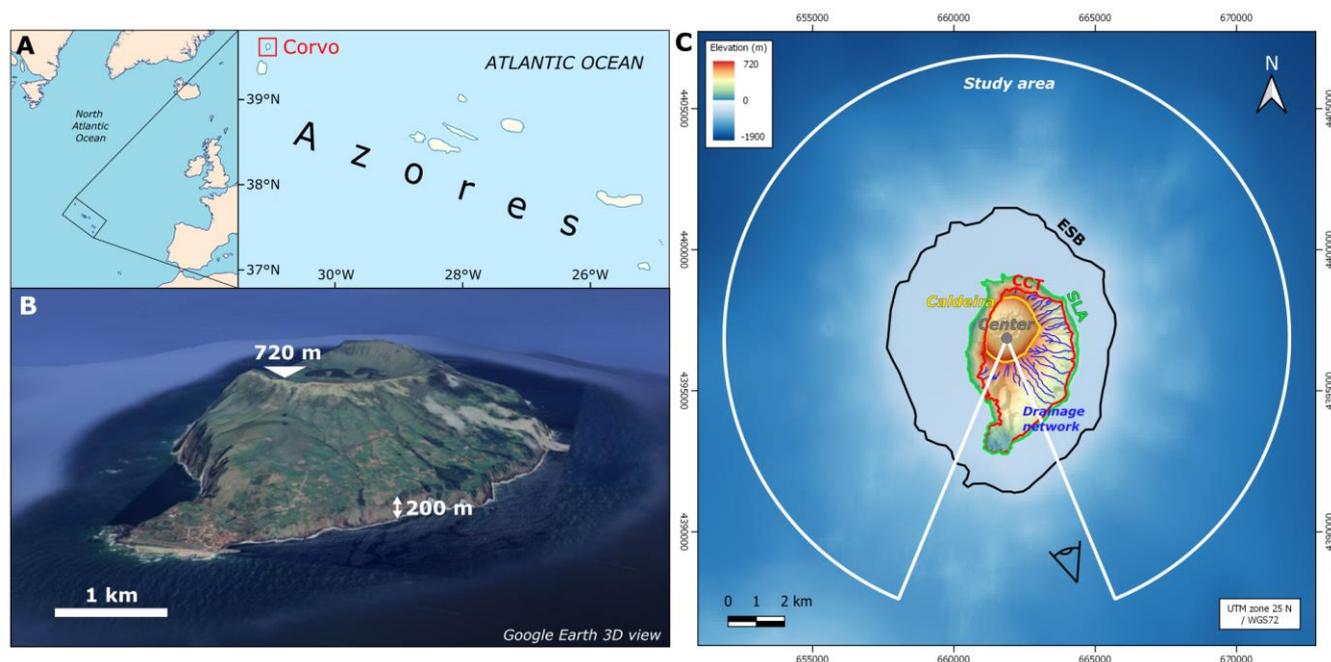
Figure 3: A: Location of Corvo Island. B: Corvo Island seen from the southeast (© Google Earth 3D view). C: Topographic shaded
325 **map of the volcanic edifice of Corvo (ASTER and EMODnet data). White line: study area. Black line: ESB. Green line: coastline, SLA. Red line: CCT. Yellow line: edges of the Central Volcano caldera. Blue lines: drainage network on the slopes of Central Volcano. Gray dot: center of the volcanic edifice.**

The insular shelf surrounding Corvo Island has a quasi-circular shape approximately 8 km in diameter, roughly centered on the Central Volcano crater (Fig. 3). The absence of large concavities on the rim of this shelf suggests that the island has not

330 experienced any major collapse since its formation, unlike neighboring islands such as Faial or Pico (Costa et al., 2015; Marques et al., 2021) and numerous volcanic edifices (Holcomb and Searle, 1991). The general aerial shape of the central volcano as well as the shape of the insular shelf therefore suggest that Corvo Island is made up of a single, radially symmetric central volcanic edifice (apart from the parasitic southern cones) with a radius of approximately 4 km (Melo et al., 2018). The presence of high coastal cliffs confirms the major role of coastal erosion in the morphological evolution of

335 Corvo. This makes Corvo Island an ideal case for testing our approach.

In order to satisfy the working hypothesis of one single, radially symmetric volcanic edifice, our study excludes the southern sector of the island, between the directions 160°N and 200°N with respect to the center of the edifice (Fig. 3), containing the younger parasitic cones. Our analysis extends up to a distance of 10 km from the center of the edifice, which corresponds approximately to the geographic boundary of the submarine edifice.

4.2 Data

The method has been designed to be broadly applicable. We consequently preferred the use of global topographic data. Therefore, we compared the results obtained with GDEM SRTM1 or ASTER topographic data, both of which have a horizontal resolution of 1 arc second, or about 30 m, which seems sufficient for Corvo.

Regarding the bathymetry, the global GEBCO data do not allow to clearly identify the contours of an insular shelf because of their insufficient horizontal resolution. As a result, we used the EMODnet database. This database covers the whole European territory, of which the Azores are part, and offers aerial and submarine topographic data around Corvo with a horizontal resolution of 50 m per pixel, which is sufficient for our analysis.

These different datasets are initially delivered in longitude/latitude in the WGS84 datum. To rectify the deformations induced by this coordinate system, we have re-projected the data into UTM (zone 25N, WGS72 datum; Fig. 3).

In order to choose the best dataset between SRTM1 and ASTER, we compared these data with the EMODnet dataset. It appears that the SRTM1 data are more accurate than the ASTER data (Kervyn et al., 2008). However, these data indicate an upward shift of several tens of meters compared to EMODnet, which breaks up the topographic continuity between these two datasets. In further detail, the SRTM1 data are quite precise but lack accuracy. In contrast, the ASTER data is noisier, indicating lower accuracy. However, the ASTER data diverge less from EMODnet than SRTM, indicating better accuracy.

In the context of our study, which is based on a surface fitting, it seems more relevant to focus on accuracy rather than precision. We therefore decided to use a combination of ASTER and EMODnet data for our analysis. This choice results in a higher uncertainty on the fit, but this is compensated by a higher reliability.

5 Results

5.1 Location of the CCT, ESB and the center of the volcanic edifice

The center of the island (lat: 39.7056° N; long: 31.1111° W), determined from the analysis of the drainage network within the CCT polygon, does not correspond precisely to the center of the Central Volcano caldera, it is located slightly more to the south (Fig. 3).

The coastal cliff top (CCT) has a complex shape, with a marked protrusion to the southeast. This shape does not appear to be centered on the defined center of the edifice; its centroid is noticeably to the southeast of it. The CCT is located between 800 m and 3000 m from the center of the edifice (from west to southeast respectively) (Fig. 3).

The shape of the Erosional Shelf Break (ESB) is more similar to a circle with a slight north-south elongation. It has a radius of approximately 4000 m and it is almost centered on the center of the edifice (Fig. 3). The mean depth of the ESB in our study area is 107.25 m below current sea level.

5.2 Topographic reconstruction

370 Figure 4 shows the radial elevation profiles of the ASTER and EMODnet data points. The radial profiles are demarcated by two point clouds with relatively low dispersion, reflecting a strong radial symmetry of the edifice. However, we notice a prominence above the point cloud roughly 1500 m north from the center of the edifice. This topographic anomaly corresponds to the northern edge of the main crater and does not seem to have been noted in previous geomorphological studies on Corvo. The parameters of the regression and associated uncertainties (equations (1) and (2)) are reported in Table

375 1. Vertical uncertainties (Δy) are of the order of $\pm$ 70 m for the aerial fit and $\pm$ 50 m for the submarine fit. The two curves intersect at a point (IE) located 3795 $\pm$ 318 m from the center of the island and 23 $\pm$ 104 m above the current sea level. As discussed previously, the IE indicates the maximum (initial) extension of the island. The IE is shown in purple in Figure 5, it is obvious that the IE is slightly internal to the ESB contour.

	a	b	c	Δa	Δb	Δc
Subaerial fit (ASTER)	1.264E+03	3.937E-04	-2.604E+02	2.422E+01	2.201E-05	3.558E+01
Submarine fit (EMODnet)	4.700E+03	2.664E-04	-1.687E+03	4.253E+01	3.063E-06	8.601E+00

380 **Table 1: Parameters and their residual standard error used in equations (1) and (2) to calculate the initial radial topographic profiles of Corvo (Fig. 4).**
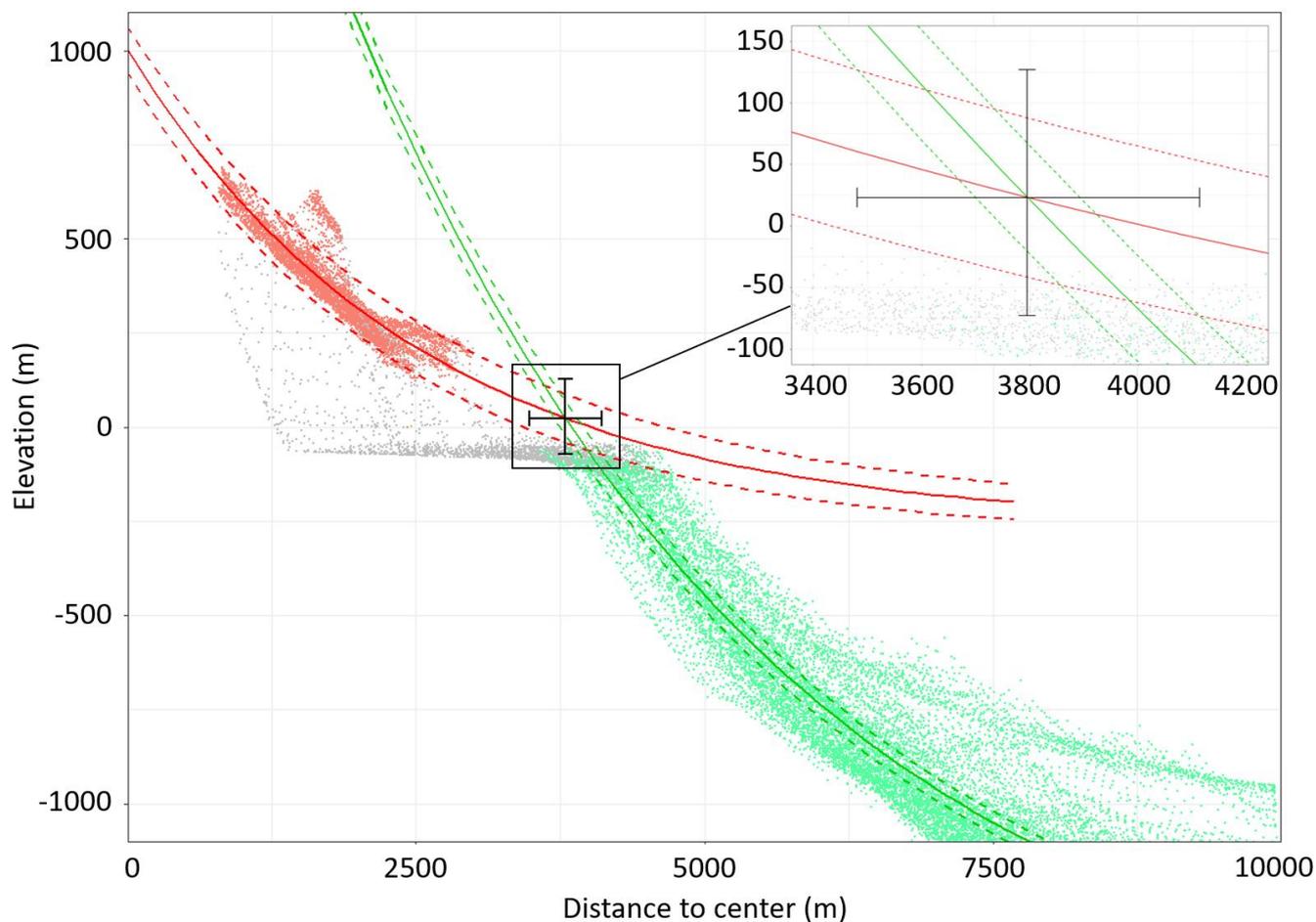
Figure 4: Elevation of the topographic data versus the distance to the center of the edifice, and the initial aerial (red) and submarine (green) radial exponential profiles reconstructed with their uncertainty domain. Red dots: representative data of the initial aerial shape; the red dots, mostly above all the others, belong to the northern sector. Green dots: representative data of the initial submarine shape. Gray dots: data in the effective coastal erosion area.
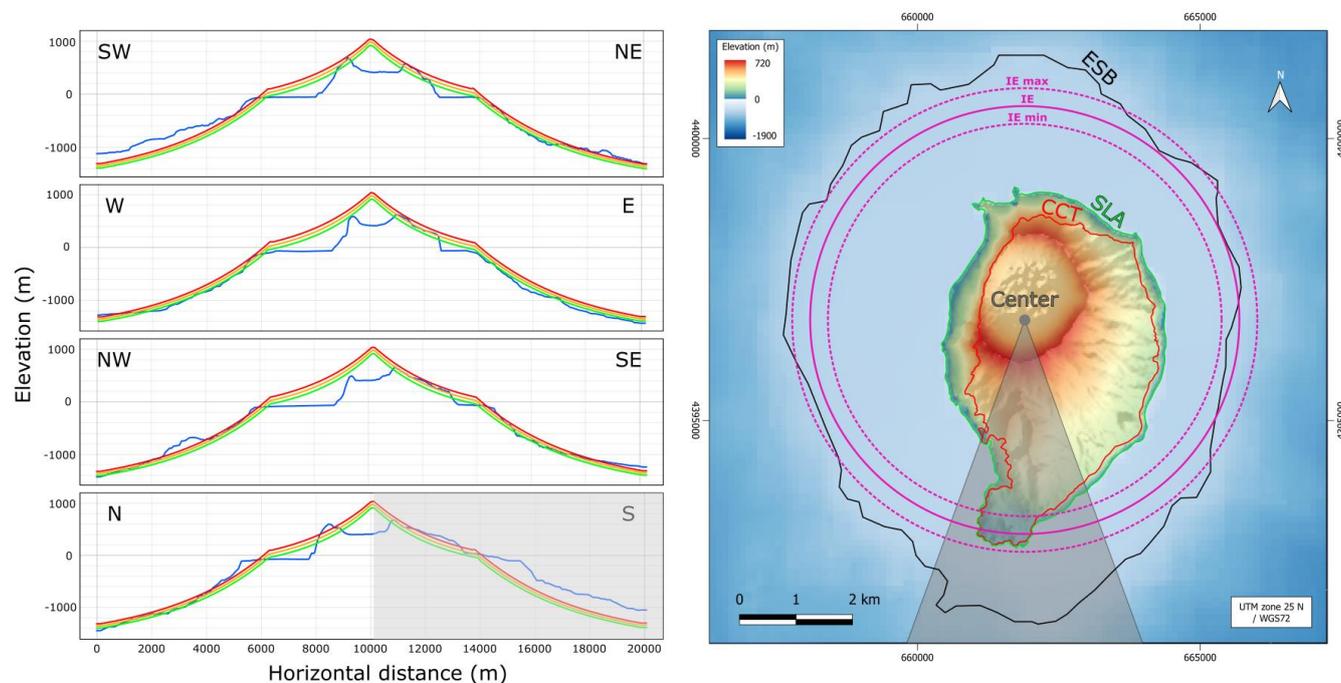
Figure 5: Left: comparison between the present-day radial topographic profiles of the Corvo volcanic edifice (blue lines) and the mean (yellow lines), minimum (green lines), and maximum (orange lines) reconstructed topographic profiles from different directions. Right: similar map to the one provided in Figure 3 showing the initial extension of the island (solid purple line) with the uncertainty values (dashed purple lines). The grey area figures the southern sector where are located volcanic progradation and which have been subsequently discarded for the analysis.

5.3 Coastal cliff retreat and eroded volume

In order to quantify the cliff retreat, we radially divided our study area into 10° sectors. For each sector, we calculated the radial horizontal distance between the mean position of the CCT and the position of the IE (Tab. 2). The result is presented as a rose diagram showing the cliff retreat in Figure 6.

sector (°)	Retreat (m)			Eroded Volume (m³)		
	Mean	Minimum	Maximum	Mean	Minimum	Maximum
0-10	1973	1659	2291	1.77E+08	1.09E+08	2.53E+08
10-20	1954	1640	2272	1.66E+08	1.01E+08	2.41E+08
20-30	1914	1600	2232	1.66E+08	9.88E+07	2.46E+08
30-40	1821	1507	2139	1.68E+08	9.94E+07	2.54E+08
40-50	1725	1411	2043	1.56E+08	8.97E+07	2.36E+08
50-60	1592	1278	1910	1.30E+08	7.17E+07	2.01E+08
60-70	1591	1277	1909	1.51E+08	8.07E+07	2.35E+08

70-80	1606	1292	1924	1.37E+08	7.16E+07	2.23E+08
80-90	1539	1225	1857	1.31E+08	7.05E+07	2.15E+08
90-100	1491	1177	1809	1.47E+08	8.15E+07	2.38E+08
100-110	1387	1073	1705	1.52E+08	7.80E+07	2.42E+08
110-120	1295	981	1613	1.29E+08	6.57E+07	2.11E+08
120-130	1227	913	1545	1.03E+08	5.37E+07	1.68E+08
130-140	1050	736	1368	7.77E+07	3.39E+07	1.31E+08
140-150	975	661	1293	6.27E+07	2.33E+07	1.15E+08
150-160	858	544	1176	3.72E+07	8.08E+06	7.67E+07
200-210	1853	1539	2171	1.63E+08	9.54E+07	2.39E+08
210-220	2119	1805	2437	1.99E+08	1.26E+08	2.80E+08
220-230	2464	2150	2782	2.34E+08	1.53E+08	3.24E+08
230-240	2772	2458	3090	2.68E+08	1.82E+08	3.64E+08
240-250	2855	2541	3173	2.86E+08	1.96E+08	3.89E+08
250-260	2964	2650	3282	3.10E+08	2.16E+08	4.14E+08
260-270	2982	2668	3300	3.27E+08	2.33E+08	4.29E+08
270-280	2994	2680	3312	3.33E+08	2.39E+08	4.35E+08
280-290	2984	2670	3302	3.33E+08	2.40E+08	4.35E+08
290-300	2963	2649	3281	3.29E+08	2.37E+08	4.31E+08
300-310	2906	2592	3224	3.28E+08	2.38E+08	4.27E+08
310-320	2835	2521	3153	3.27E+08	2.37E+08	4.23E+08
320-330	2733	2419	3051	3.17E+08	2.29E+08	4.13E+08
330-340	2593	2279	2911	2.90E+08	2.04E+08	3.83E+08
340-350	2448	2134	2766	2.23E+08	1.42E+08	3.14E+08
350-0	2179	1865	2497	1.88E+08	1.19E+08	2.67E+08

Table 2: Coastal cliff retreat and eroded volume calculated by 10° sectors around Corvo Island.
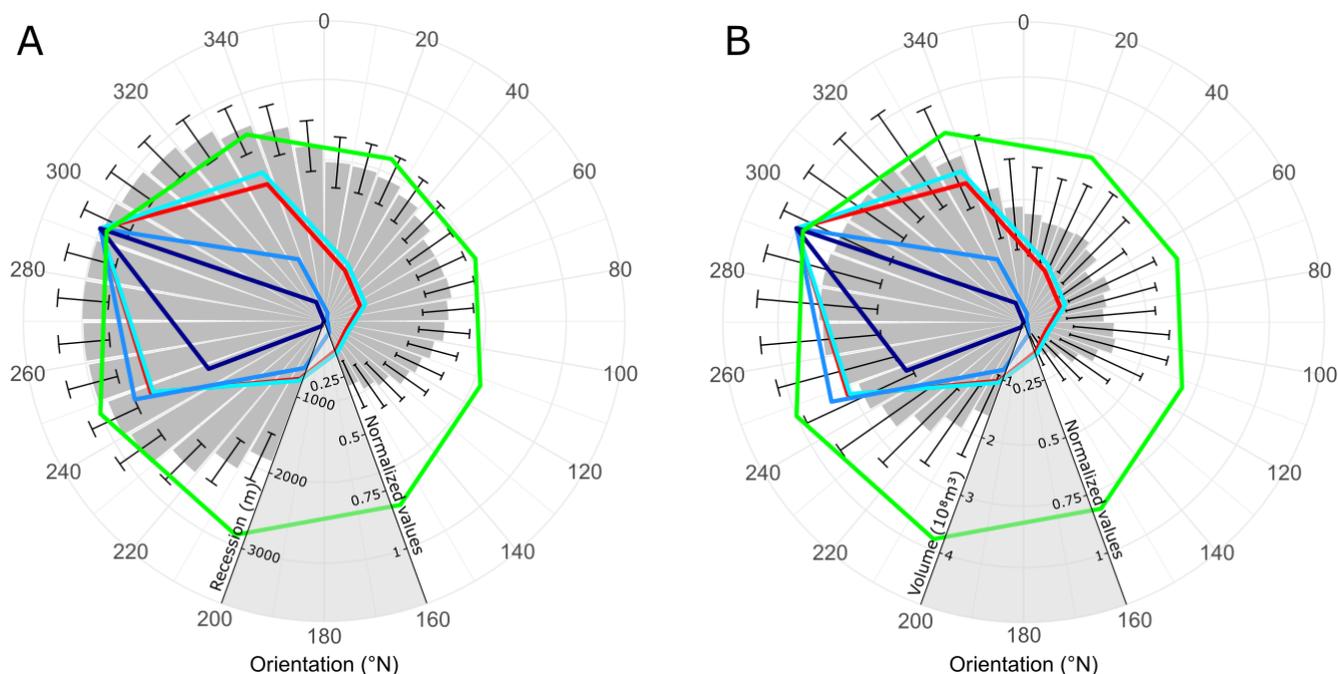
Figure 6: Quantification of the total coastal erosion with respect to direction. A: Total coastal cliff retreat (distance IE-CCT). B: Total eroded volume. The wave data from Rusu and Guedes Soares (2012) are shown in color and in values normalized by their maximum (see Tab. 2 and 3 for the detailed actual values). Red: spatial distribution for the waves. Light blue: spatial distribution for the waves with Hs < 5 m. Blue: spatial distribution for the waves with 5 m < Hs < 10 m. Dark blue: spatial distribution for the waves with Hs > 10 m. Green: mean Hs of the waves.

We also quantified the eroded volume as the difference between the reconstructed initial topography and the current topography (Tab. 2). The eroded volume was calculated inside the area between the current horizontal position of the CCT and the current mean depth of the ESB (cf. methods). The calculated volume is only counted when the reconstructed initial topography is above the current topography. Over the study area, i.e. the southern sector of the island is excluded, the total eroded volume by the sea is evaluated as roughly 6.5 ± 2.7 km^3. The corresponding surface area eroded by the sea is approximately 37.2 ± 3.6 km^2 (area between the CCT and ESB). Compared to the current Corvo Island surface area above the cliffs without the southern sector spanning 9.1 km2, we infer that the island has lost roughly 80% of its surface area following coastal erosion. The sectorization of this eroded volume provide an insight into the erosion distribution (Tab. 2, Fig. 6).

6 Discussion

6.1 Method robustness, limitations and improvements

Following the same method as previous works (e.g. Karátson et al., 2016) but complementing it with the consideration of the submarine part of the edifice, the reconstructed initial shape of Corvo Island does a good job of enveloping the current shape

of the island (Fig. 5). However, this reconstruction is less convincing in the northern sector where the initial reconstructed elevation lies below the present-day elevation regardless of whether its aerial or submarine parts are considered. Our method

420 allows to precisely quantify the ±1σ uncertainties associated with the calculation of the fits (Tab. 1). These uncertainties also allow us to quantify the uncertainties associated with the coastal cliff retreat and eroded volumes (Tab. 2). The uncertainties in the cliff retreat range from ±10% in the most eroded areas (western sectors) to ±37% in the least eroded areas (southeastern sectors). The uncertainties in the eroded volumes range from ±28% to -78/+106%, respectively. Thus, the best sectors have an uncertainty of close to one quarter. This error is comparable with the errors associated with annual to decadal

425 measurements (e.g. Moses and Robinson, 2011; Earlie et al., 2013; Young, 2018). The uncertainty in the total eroded volume is ±42% (slightly better than published values; cf. Averes et al., 2021; Regard et al., 2022). These uncertainties depend on the number of points used to calculate the fit. Therefore, our method is deemed to be more robust for higher resolution data or for larger islands.

Our approach has the advantage of providing usable results from a simple method that can be generalized to other islands.
430 However, some important limitations remain.

First of all, our method requires that the initial shape of the volcanic edifice or a part of it has radial symmetry. This hypothesis can be easily tested, for example by dividing the island into different dials and by comparing the predicted center (by applying our method) of each dial with the others. In the case that the symmetry does not hold for the whole island, or in case of multiple volcanic edifices, our approach can be still applied independently for some selected dials. Moreover, by

435 fitting the point cloud in the aerial part of the island, we do not take the fluvial erosion into account and therefore the elevation of the fitted topography may be lower than the oldest, original, island surface. This strategy is relevant for islands that are similar to Corvo, with relatively well-preserved volcanic morphology. For deeply incised islands, depending on available geological (lava surface) or topographical (relicts of volcano surface) data, other strategies can be chosen by selecting the points belonging to the oldest reference surface (Lahitte et al., 2012; Germa et al., 2015) without changing the

440 general approach of our method.

The method could also be adapted by considering more complex initial shapes. For example, Favalli et al. (2014) showed that it is possible to work with elliptical or hyperelliptical based cones and Gaussian topographic profiles to reconstruct the initial shape of terrestrial volcanoes. These alternatives must be evaluated for each specific case by choosing the topographic model that better fits the data. These choices could lead to second-order variations in the results. Adapting the topographic

445 model in each case could be an added bonus to our method, for which the main improvement consists of incorporating aerial and submarine topographic profiles, compared to previous works based on aerial data only (Hildenbrand et al., 2008; Lahitte et al., 2012; Germa et al., 2010, 2015; Ricci et al., 2015a, 2015b; Karátson et al., 2016).

Another limitation is the requirement of high-resolution bathymetric data around the island to accurately map the ESB, which is hardly available for all volcanic islands. Moreover, the unknown volume of sediment deposited on the shelf

450 constitutes another uncertainty in the calculation of the eroded volume. Sedimentation raises the shelf bathymetry relative to

the actual depth of the bedrock, possibly leading to an underestimation of the total eroded volume from the bedrock. However, if we are interested in the net material removal from the island to the deep ocean, this is not a problem.

Lastly, our method allows for the quantification of the average erosion and vertical movement rates integrated over the age of the island, but cannot be used to identify, even qualitatively, the variations of these parameters over time.

6.2 Coastal erosion rates and vertical dynamics

In accordance with the suggestions of Melo et al. (2018), we obtain an initial aerial edifice with a radius of nearly 4 km and a height close to 1 km; we assume that the caldera formed in a second stage. The reconstruction of this pre-erosion shape allows us to evaluate a total coastal cliff retreat ranging from 550 to 3300 m. The six-fold variation in the coastal cliff retreat depends on the sector: the largest values stand for the sectors to the west and northwest. Considering that the age of this reconstructed shape corresponds to the age of Central Volcano, 0.43 ± 0.34 Ma, the large uncertainty associated with this age is reflected in the large uncertainty on the integrated mean coastal erosion rates. Depending on the sector, erosion rates range 0.7-4.3 mm/yr and 6-37 mm/yr, respectively, for the maximum and minimum age bounds of 770 ka and 90 ka. Our cliff rate evaluation varies by a factor of 8 depending on the age adopted. On the other hand, it is possible that the coastal cliff retreat is restricted to interglacial periods when the sea level is close to the present one (e.g. Ramalho et al., 2013; Ye et al., 2013). Since these periods correspond to approximately 10% of the time since the formation of the island, the cliff retreat rates should be multiplied by 10, i.e. erosion rates between 7 and 370 mm/yr (depending on the sector and on the uncertainty). Lastly, these long-term coastal erosion rates are consistent with the orders of magnitude of short-term coastal erosion rates measured on basalts, i.e. 10 to 100 mm/year (Prémaillon et al., 2018), showing that our method provides realistic results, at least in the case of Corvo Island.

In addition to being able to quantify the total coastal erosion, the reconstruction of the initial shape of Corvo Island allows us to obtain the elevation of the junction relative to the current sea level between the aerial and submarine profiles, which is assumed to be the initial extension (IE) of the island. The IE is 23 ± 104 m above current sea level. This value, despite its large uncertainty is comparable to the difference between the theoretical depth of -130 m in the absence of vertical movements of the ESB (Shepard, 1973; Trenhaile, 2001; Quartau et al., 2010) and its actual value of -107.25 m. This suggests that Corvo Island could have possibly experienced a mean uplift of approximately 20 m since the formation of Central Volcano. However, given the large vertical uncertainty, estimating a total uplift value would be too uncertain to be further discussed. Moreover, a total uplift value can hide important variations in the vertical movement through time. For example, this is the case for Santa Maria Island, as well as in the Azores archipelago, which experienced a period of subsidence before experiencing a major uplift (Ramalho et al., 2017). In addition, the large uncertainty in the age of Central Volcano means that is not possible to accurately estimate the sea level at the time coastal erosion started. Consequently, it remains difficult to assess the effect of a possible uplift on the coastal erosion rate.

It is worth noting that the topographic anomaly observed in Figure 4 corresponds to the northern sector. There, the aerial elevation is higher than elsewhere on the island with respect to the radial symmetry, meanwhile the insular shelf is also

wider. This indicates a vertical and horizontal protrusion. Together with the protrusion caused by the younger volcanic
485 edifice in the southern sector of the island, these protrusions give the total edifice a slight elongation along the north-south
axis. Similarly to the southern protrusion of volcanic origin, it is conceivable that the northern one is also due to volcanic
processes. We suggest that it is older than Central Volcano because it is almost totally eroded by the sea, leaving a wider
insular shelf in this sector. However, geological studies by Dias (2001) and França et al. (2002, 2006) do not seem to support
this. Another solution to explain this elongation is a tectonic origin. The deformation of the edifice along its north-south axis
490 during its evolution would be due to the dynamics of the Mid-Atlantic Ridge (Pueyo Anchuela et al., 2006). This slight
elongation is not considered in our working hypotheses; if true, it would imply that the cliff retreat and eroded volume values
in the northern sector are underestimated.

6.3 Comparison with available wave data

In order to perform an early analysis of the factors controlling the long-term coastal erosion, wave data from Rusu and
495 Guedes Soares (2012) (calculated from the KNMI/ERA-40 Wave Atlas) were compared with the directional coastal cliff
retreat and eroded volume data in Figure 6. These wave data are calculated from a global wave model (Tab. 3) and provide
information, per 45° quadrant, about: the directional distribution of the waves, the distribution and average of the significant
wave height (Hs). To observe the effect of significant wave height, we present wave data subdivided into three classes: Hs <
5 m, 5 m < Hs < 10 m and Hs > 10 m (Tab. 3 and Fig. 6).

500

sector (°)	Wave frequency (%)	Hs distribution (%) for each sector			Mean Hs (m)
		0 m < Hs < 5 m	5 m < Hs < 10 m	Hs >10 m	
0-45	7	97.89	2.12	0.00	2.33
45-90	5	99.01	0.98	0.00	2.17
90-135	3	97.69	2.30	0.00	2.24
135-180	4	94.69	5.30	0.00	2.64
180-225	8	89.50	10.48	0.03	3.07
225-270	24	85.65	14.11	0.24	3.21
270-315	31	86.75	12.91	0.36	3.12
315-360	19	94.11	5.83	0.05	2.68

Table 3: Wave data from Rusu and Guedes Soares (2012) used for this study. Hs: significant wave height (m).

There appears to be a clear spatial correlation between the distribution of the waves and cliff retreat or the eroded volumes.
There is also a correlation between the mean significant wave height and cliff retreat, but this appears to be less marked.
These correlations are analyzed by plotting the values of our results against the values given by Rusu and Guedes Soares
505 (2012), and by calculating their correlation coefficients (ρ) (Fig. 7). It appears from the correlations (Fig. 7) as well as the

visual inception (Fig. 6) that cliff retreat and eroded volume are much better correlated with the distribution of the waves rather than with the mean wave height. In particular, the distribution of small waves (Hs < 5 m) is better correlated with cliff retreat and eroded volume than those of large waves (5 m < Hs < 10 m) and even more than those of very large waves (Hs > 10 m). Thus, contrary to the assertion by Anderson and Anderson (2010) and Ramalho et al. (2013) that mainly storm waves

510 control coastal erosion, our results would indicate a stronger control by smaller and more usual waves, in accordance with the conclusions of Huppert et al. (2020).
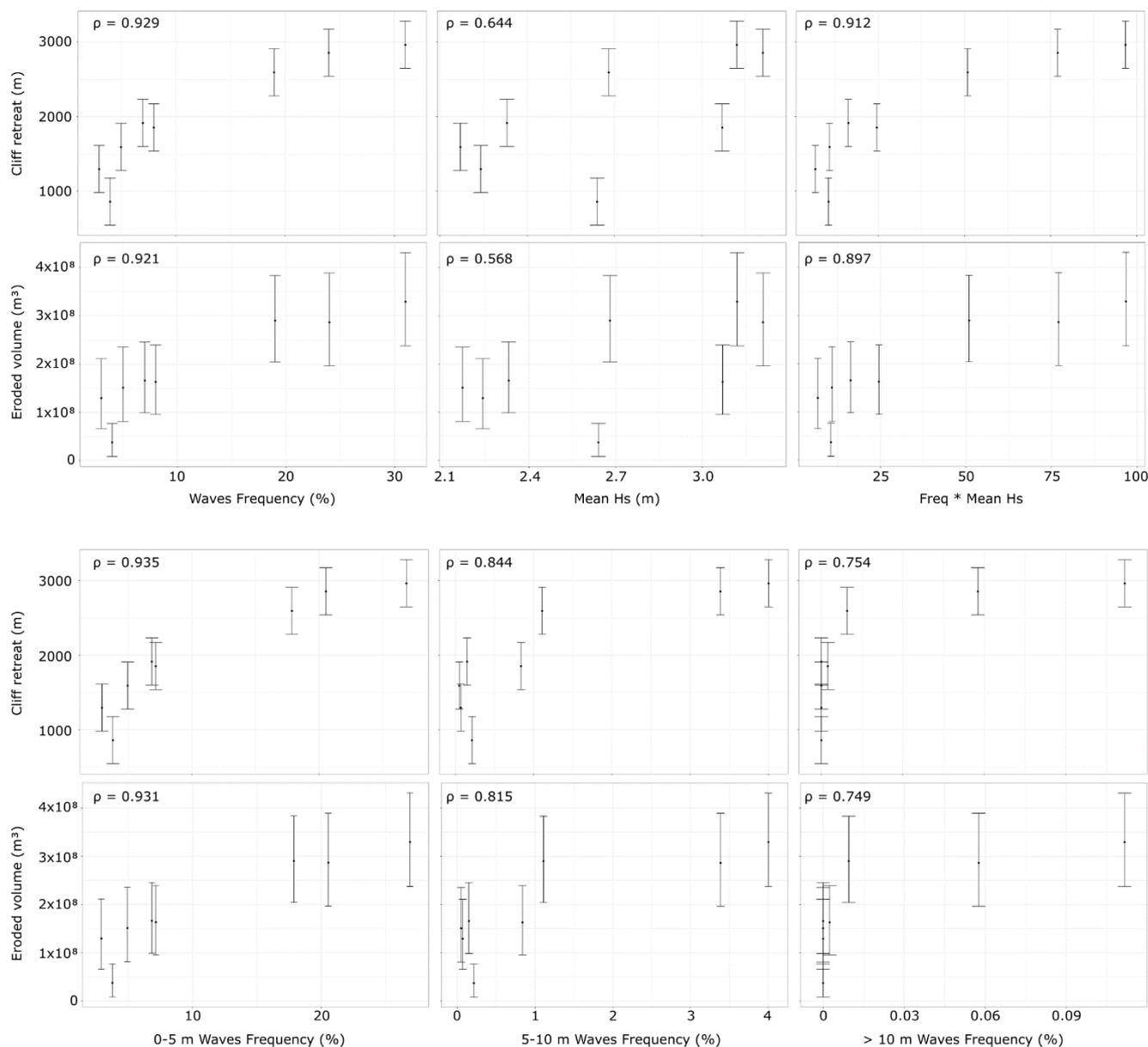
Figure 7: Quantification of the correlations (ρ) between the coastal cliff retreat and eroded volume, and the mean significant wave height (Hs) and frequency.

515 Lastly, it appears that the maximum wave activity, which is located between 240°N and 340°N, is opposite to the locus of the minimum cliff retreat and eroded volume, which is located between 120°N and 160°N. This minimum coastal erosion could be due to the protection that the island, and the lava delta in the southern sector in particular, offers against the dominant swell via a shading effect.

In view of the correlation between waves and coastal erosion, despite the uncertainties on the absolute values of the coastal
520 cliff retreat and eroded volume, the method seems capable of accurately capturing the spatial variations of this erosion around the island. These results open up promising perspectives that must be confirmed by the application of this method to other volcanic islands.

7 Conclusions

We have developed a method to reconstruct the initial shape of simple volcanic islands from aerial and submarine
525 topographic data. It allows to spatially quantify the total coastal erosion integrated over the age of the maximum island extension.

Applying this method to the Corvo Island in the Azores archipelago, we calculated that, at its maximum extension, the radius of the island was approximately 3.8 km for a peak elevation of roughly 1 km. Comparing this reconstructed shape with the current shape, we estimated that the island had lost a volume of about 6.5 ± 2.7 km^3 and an area of about 37.2 ± 3.6 km^2
530 along its coast, due to coastal erosion; it corresponds to more than three quarters of its initial surface. We estimated that the cliff retreated by 550 m to 3300 m in the most exposed sectors. The large uncertainty on the age of the island means that it is not possible to calculate an accurate retreat rate; it is comprised between 7 and 370 mm/year, i.e. equivalent in magnitude to short-term observations on similar lithologies. Lastly, the comparison of the cliff retreat and eroded volume values with the available wave data shows a strong spatial correlation between wave frequency and coastal erosion. Furthermore, contrary to
535 the assertion of previous researchers, moderate but frequent waves appear to have a greater control on coastal erosion than storm waves.

Similar studies on other volcanic islands could consolidate and enrich our method, provide new results for different lithologies and ages, and improve the correlations observed in this study.

Data availability

540 Raw data for our study come from open access topographic data. They can be freely downloaded from the website https://search.earthdata.nasa.gov/search for ASTER data and from the website https://portal.emodnet-bathymetry.eu for

EMODnet data. The main derived data are presented in tables 1 and 2. All products from these data can be provided by the corresponding authors upon request.

Author contributions

545 RB developed the method, performed the study and wrote the manuscript with contributions from VR and SC.

Competing interests

The authors declare that they have no conflict of interest.

References

Anderson, Densmore, Ellis, 1999. The generation and degradation of marine terraces. Basin Res. 11, 7–19.
550 https://doi.org/10.1046/j.1365-2117.1999.00085.x

Anderson, R.S., Anderson, S.P., 2010. Geomorphology: the mechanics and chemistry of landscapes. Cambridge University Press.

Averes, T., Hofstede, J.L.A., Hinrichsen, A., Reimers, H.-C., Winter, C., 2021. Cliff Retreat Contribution to the Littoral Sediment Budget along the Baltic Sea Coastline of Schleswig-Holstein, Germany. J. Mar. Sci. Eng. 9, 870.
555 https://doi.org/10.3390/jmse9080870

Ávila, S.P., Santos, A.C., Penteado, A.M., Rodrigues, A.M., Quintino, I., Machado, M.I., 2005. The molluscs of the intertidal algal turf in the Azores. Los moluscos del cesped algal intermareale en Azores.

Benumof, B.T., Storlazzi, C.D., Seymour, R.J., Griggs, G.B., 2000. The Relationship between Incident Wave Energy and Seacliff Erosion Rates: San Diego County, California. J. Coast. Res. 16, 1162–1178.

560 Bintanja, R., van de Wal, R.S.W., 2008. North American ice-sheet dynamics and the onset of 100,000-year glacial cycles. Nature 454, 869–872. https://doi.org/10.1038/nature07158

Bird, E.C., 2011. Coastal geomorphology: an introduction. John Wiley & Sons.

Buchanan, D.H., Naylor, L.A., Hurst, M.D., Stephenson, W.J., 2020. Erosion of rocky shore platforms by block detachment from layered stratigraphy. Earth Surf. Process. Landf. 45, 1028–1037. https://doi.org/10.1002/esp.4797

565   Catalão, J., Catita, C., Miranda, J., Dias, J., 2002. Photogrammetric analysis of the coastal erosion in the Algarve (Portugal)/Analyse photogrammétrique de l'érosion côtiere en Algarve (Portugal). Géomorphologie Relief Process. Environ. 8, 119–126.

Chang, Y.-C., Mitchell, N.C., Quartau, R., 2021. Landslides in the Upper Submarine Slopes of Volcanic Islands: The Central Azores. Geochem. Geophys. Geosystems 22, e2021GC009833. https://doi.org/10.1029/2021GC009833

570   Costa, A.C.G., Hildenbrand, A., Marques, F.O., Sibrant, A.L.R., Santos de Campos, A., 2015. Catastrophic flank collapses and slumping in Pico Island during the last 130 kyr (Pico-Faial ridge, Azores Triple Junction). J. Volcanol. Geotherm. Res. 302, 33–46. https://doi.org/10.1016/j.jvolgeores.2015.06.008

Costa, S., Maquaire, O., Letortu, P., Thirard, G., Compain, V., Roulland, T., Medjkane, M., Davidson, R., Graff, K., Lissak, C., 2019. Sedimentary Coastal cliffs of Normandy: modalities and quantification of retreat. J. Coast. Res. 88, 46–60.

575   DePaolo, D.J., Stolper, E.M., 1996. Models of Hawaiian volcano growth and plume structure: Implications of results from the Hawaii Scientific Drilling Project. J. Geophys. Res. Solid Earth 101, 11643–11654. https://doi.org/10.1029/96JB00070

Dewez, T.J., Rohmer, J., Regard, V., Cnudde, C., 2013. Probabilistic coastal cliff collapse hazard from repeated terrestrial laser surveys: case study from Mesnil Val (Normandy, northern France). J. Coast. Res. 702–707.

Dias, J.L.F., 2001. Geologia e tectónica da ilha do Corvo (Açores-Portugal): Contributos para o ordenamento do espaço
580   físico.

Dias, J.M.A., Neal, W.J., 1992. Sea Cliff Retreat in Southern Portugal: Profiles, Processes, and Problems. J. Coast. Res. 8, 641–654.

Dornbusch, U., Robinson, D.A., Moses, C.A., Williams, R.B., 2008. Temporal and spatial variations of chalk cliff retreat in East Sussex, 1873 to 2001. Mar. Geol. 249, 271–282.

585   Duguet, T., Duperret, A., Costa, S., Regard, V., Maillet, G., 2021. Coastal chalk cliff retreat rates during the Holocene, inferred from submarine platform morphology and cosmogenic exposure along the Normandy coast (NW France). Mar. Geol. 433, 106405.

Earlie, C., Masselink, G., Russell, P., Shail, R., 2013. Sensitivity analysis of the methodology for quantifying cliff erosion using airborne LiDAR–examples from Cornwall, UK. J. Coast. Res. 470–475.

590 Favalli, M., Karátson, D., Yepes, J., Nannipieri, L., 2014. Surface fitting in geomorphology — Examples for regular-shaped volcanic landforms. Geomorphology 221, 139–149. https://doi.org/10.1016/j.geomorph.2014.06.009

Ferrer-Valero, N., Hernández-Calvento, L., 2020. Coastal geomorphic chronosequences across broad spatiotemporal scales. Metrical observations from the Cape Verde hotspot. Earth Surf. Process. Landf. 45, 511–525. https://doi.org/10.1002/esp.4738

595 França, Z., Lago San José, M., Nunes, J., Gale, C., Forjaz, V.-H., Anchuela, O., Arranz Yagüe, E., 2006. Geochemistry of alkaline basalts of Corvo Island (Azores, Portugal): Preliminary data. Geogaceta 40, 87–90.

França, Z., Nunes, J., Cruz, J., Duarte, J.F., Forjaz, V.-H., 2002. Preliminary study of the Corvo Island volcanism, Azores. 3° Assem. Luso-Esp. Geod. E Geofísica S09 727–730.

Germa, A., Lahitte, P., Quidelleur, X., 2015. Construction and destruction of Mont Pelée volcano: Volumes and rates 600 constrained from a geomorphological model of evolution. J. Geophys. Res. Earth Surf. 120, 1206–1226. https://doi.org/10.1002/2014JF003355

Germa, A., Quidelleur, X., Labanieh, S., Lahitte, P., Chauvel, C., 2010. The eruptive history of Morne Jacob volcano (Martinique Island, French West Indies): Geochronology, geomorphology and geochemistry of the earliest volcanism in the recent Lesser Antilles arc. J. Volcanol. Geotherm. Res. 198, 297–310. https://doi.org/10.1016/j.jvolgeores.2010.09.013

605 Gibb, J.G., 1978. Rates of coastal erosion and accretion in New Zealand. N. Z. J. Mar. Freshw. Res. 12, 429–456.

Grant, P.J., 1981. Recently increased tropical cyclone activity and inferences concerning coastal erosion and inland hydrological regimes in New Zealand and eastern Australia. Clim. Change 3, 317–332.

Hapke, C.J., Reid, D., Richmond, B., 2009. Rates and trends of coastal change in California and the regional behavior of the beach and cliff system. J. Coast. Res. 25, 603–615.

610 Hildenbrand, A., Gillot, P.-Y., Marlin, C., 2008. Geomorphological study of long-term erosion on a tropical volcanic ocean island: Tahiti-Nui (French Polynesia). Geomorphology 93, 460–481. https://doi.org/10.1016/j.geomorph.2007.03.012

Holcomb, R.T., Searle, R.C., 1991. Large landslides from oceanic volcanoes. Mar. Georesources Geotechnol. 10, 19–32.

Huppert, K.L., Perron, J.T., Ashton, A.D., 2020. The influence of wave power on bedrock sea-cliff erosion in the Hawaiian Islands. Geology 48, 499–503. https://doi.org/10.1130/G47113.1

615 Hurst, M.D., Rood, D.H., Ellis, M.A., Anderson, R.S., Dornbusch, U., 2016. Recent acceleration in coastal cliff retreat rates on the south coast of Great Britain. Proc. Natl. Acad. Sci. 113, 13336–13341.

Karátson, D., Favalli, M., Tarquini, S., Fornaciai, A., Wörner, G., 2010. The regular shape of stratovolcanoes: A DEM-based morphometrical approach. J. Volcanol. Geotherm. Res. 193, 171–181. https://doi.org/10.1016/j.jvolgeores.2010.03.012

Karátson, D., Yepes, J., Favalli, M., Rodríguez-Peces, M.J., Fornaciai, A., 2016. Reconstructing eroded paleovolcanoes on
620 Gran Canaria, Canary Islands, using advanced geomorphometry. Geomorphology 253, 123–134. https://doi.org/10.1016/j.geomorph.2015.10.004

Kennedy, D.M., Dickson, M.E., 2007. Cliffed coasts of New Zealand: perspectives and future directions. J. R. Soc. N. Z. 37, 41–57.

Kervyn, M., Ernst, G.G.J., Goossens, R., Jacobs, P., 2008. Mapping volcano topography with remote sensing: ASTER vs.
625 SRTM. Int. J. Remote Sens. 29, 6515–6538. https://doi.org/10.1080/01431160802167949

Lahitte, P., Samper, A., Quidelleur, X., 2012. DEM-based reconstruction of southern Basse-Terre volcanoes (Guadeloupe archipelago, FWI): Contribution to the Lesser Antilles Arc construction rates and magma production. Geomorphology, Volcano Geomorphology: landforms, processes and hazards 136, 148–164. https://doi.org/10.1016/j.geomorph.2011.04.008

Landemaine, V., 2016. Érosion des sols et transferts sédimentaires sur les bassins versants de l'Ouest du Bassin de Paris :
630 analyse, quantification et modélisation à l'échelle pluriannuelle (phdthesis). Normandie Université.

Lavigne, F., Degeai, J.-P., Komorowski, J.-C., Guillet, S., Robert, V., Lahitte, P., Oppenheimer, C., Stoffel, M., Vidal, C.M., Pratomo, I., 2013. Source of the great AD 1257 mystery eruption unveiled, Samalas volcano, Rinjani Volcanic Complex, Indonesia. Proc. Natl. Acad. Sci. 110, 16742–16747.

Letortu, P., Costa, S., Maquaire, O., Delacourt, C., Augereau, E., Davidson, R., Suanez, S., Nabucet, J., 2015. Retreat rates,
635 modalities and agents responsible for erosion along the coastal chalk cliffs of Upper Normandy: The contribution of terrestrial laser scanning. Geomorphology 245, 3–14.

Lim, M., Rosser, N.J., Allison, R.J., Petley, D.N., 2010. Erosional processes in the hard rock coastal cliffs at Staithes, North Yorkshire. Geomorphology 114, 12–21.

Lipman, P.W., 1995. Declining growth of Mauna Loa during the last 100,000 years: Rates of lava accumulation vs.
640 gravitational subsidence, in: Rhodes, J.M., Lockwood, J.P. (Eds.), Geophysical Monograph Series. American Geophysical Union, Washington, D. C., pp. 45–80. https://doi.org/10.1029/GM092p0045

Marques, F.M.S.F., Matildes, R., Redweik, P., 2013. Sea cliff instability susceptibility at regional scale: a statistically based assessment in the southern Algarve, Portugal. Nat. Hazards Earth Syst. Sci. 13, 3185–3203. https://doi.org/10.5194/nhess-13-3185-2013

645 Marques, F.O., Catalão, J., Hübscher, C., Costa, A.C.G., Hildenbrand, A., Zeyen, H., Nomikou, P., Lebas, E., Zanon, V., 2021. The shaping of a volcanic ridge in a tectonically active setting: The Pico-Faial Ridge in the Azores Triple Junction. Geomorphology 378, 107612. https://doi.org/10.1016/j.geomorph.2021.107612

Melo, C.S., Ramalho, R.S., Quartau, R., Hipólito, A., Gil, A., Borges, P.A., Cardigos, F., Ávila, S.P., Madeira, J., Gaspar, J.L., 2018. Genesis and morphological evolution of coastal talus-platforms (fajãs) with lagoons: The case study of the newly-
650 formed Fajã dos Milagres (Corvo Island, Azores). Geomorphology 310, 138–152. https://doi.org/10.1016/j.geomorph.2018.03.006

Menard, H., 1986. Islands–Scientific American Books. N. Y. N. Y. USA.

Menard, H.W., 1983. Insular erosion, isostasy, and subsidence. Science 220, 913–918.

Micallef, A., Marchis, R., Saadatkhah, N., Pondthai, P., Everett, M.E., Avram, A., Timar-Gabor, A., Cohen, D., Preca
655 Trapani, R., Weymer, B.A., 2021. Groundwater erosion of coastal gullies along the Canterbury coast (New Zealand): A rapid and episodic process controlled by rainfall intensity and substrate variability. Earth Surf. Dyn. 9, 1–18.

Milliman, J.D., Farnsworth, K.L., 2013. River discharge to the coastal ocean: a global synthesis. Cambridge University Press.

Mitchell, N.C., Masson, D.G., Watts, A.B., Gee, M.J., Urgeles, R., 2002. The morphology of the submarine flanks of
660 volcanic ocean islands: A comparative study of the Canary and Hawaiian hotspot islands. J. Volcanol. Geotherm. Res. 115, 83–107.

Moses, C., Robinson, D., 2011. Chalk coast dynamics: Implications for understanding rock coast evolution. Earth-Sci. Rev. 109, 63–73.

Ng, K., Borges, P., Phillips, M.R., Medeiros, A., Calado, H., 2019. An integrated coastal vulnerability approach to small
665 islands: The Azores case. Sci. Total Environ. 690, 1218–1227. https://doi.org/10.1016/j.scitotenv.2019.07.013

Pacheco, J., Ferreira, T., Queiroz, G., Wallenstein, N., Coutinho, R., Cruz, J., Pimentel, A., Silva, R., Gaspar, J., Goulart, C., 2013. Notas sobre a geologia do arquipélago dos Açores, in: Geologia de Portugal. pp. 596–690.

Peterson, D.W., Moore, R.B., 1987. Geologic history and evolution of geologic concepts, in: Island of Hawaii. pp. 149–189.

Prémaillon, M., Dewez, T.J.B., Regard, V., Rosser, N.J., Carretier, S., Guillen, L., 2021. Conceptual model of fracture-limited sea cliff erosion: Erosion of the seaward tilted flyschs of Socoa, Basque Country, France. Earth Surf. Process. Landf. 46, 2690–2709. https://doi.org/10.1002/esp.5201

Prémaillon, M., Regard, V., Dewez, T.J.B., Auda, Y., 2018. GlobR2C2 (Global Recession Rates of Coastal Cliffs): a global relational database to investigate coastal rocky cliff erosion rate variations. Earth Surf. Dyn. 6, 651–668. https://doi.org/10.5194/esurf-6-651-2018

Pueyo Anchuela, Ó., Gil Imaz, A., Lago San José, M., França, Z., Galé, C., 2006. Magma flow directions in Azores basaltic dykes from AMS data: preliminary results from Corvo island.

Quartau, R., Hipólito, A., Romagnoli, C., Casalbore, D., Madeira, J., Tempera, F., Roque, C., Chiocci, F.L., 2014. The morphology of insular shelves as a key for understanding the geological evolution of volcanic islands: Insights from Terceira Island (Azores). Geochem. Geophys. Geosystems 15, 1801–1826. https://doi.org/10.1002/2014GC005248

Quartau, R., Tempera, F., Mitchell, N.C., Pinheiro, L.M., Duarte, H., Brito, P.O., Bates, C.R., Monteiro, J.H., 2012. Morphology of the Faial Island shelf (Azores): The interplay between volcanic, erosional, depositional, tectonic and mass-wasting processes. Geochem. Geophys. Geosystems 13. https://doi.org/10.1029/2011GC003987

Quartau, R., Trenhaile, A.S., Mitchell, N.C., Tempera, F., 2010. Development of volcanic insular shelves: Insights from observations and modelling of Faial Island in the Azores Archipelago. Mar. Geol. 275, 66–83. https://doi.org/10.1016/j.margeo.2010.04.008

Quartau, R., Trenhaile, A.S., Ramalho, R.S., Mitchell, N.C., 2018. The role of subsidence in shelf widening around ocean island volcanoes: Insights from observed morphology and modeling. Earth Planet. Sci. Lett. 498, 408–417. https://doi.org/10.1016/j.epsl.2018.07.007

Rachold, V., Grigoriev, M.N., Are, F.E., Solomon, S., Reimnitz, E., Kassens, H., Antonow, M., 2000. Coastal erosion vs riverine sediment discharge in the Arctic Shelf seas. Int. J. Earth Sci. 89, 450–460.

Raimbault, C., Duperret, A., Regard, V., Molliex, S., Wyns, R., Authemayou, C., Le Gall, B., 2018. Quaternary geomorphological evolution of a granitic shore platform constrained by in situ 10Be concentrations, Penmarc'h, SW Brittany, France. Mar. Geol. 395, 33–47.

Ramalho, R.S., Helffrich, G., Madeira, J., Cosca, M., Thomas, C., Quartau, R., Hipólito, A., Rovere, A., Hearty, P.J., Ávila, S.P., 2017. Emergence and evolution of Santa Maria Island (Azores)—The conundrum of uplifted islands revisited. Bulletin 129, 372–390.

Ramalho, R.S., Quartau, R., Trenhaile, A.S., Mitchell, N.C., Woodroffe, C.D., Ávila, S.P., 2013. Coastal evolution on volcanic oceanic islands: A complex interplay between volcanism, erosion, sedimentation, sea-level change and biogenic production. Earth-Sci. Rev. 127, 140–170. https://doi.org/10.1016/j.earscirev.2013.10.007

Regard, V., Prémaillon, M., Dewez, T.J.B., Carretier, S., Jeandel, C., Godderis, Y., Bonnet, S., Schott, J., Pedoja, K., Martinod, J., Viers, J., Fabre, S., 2022. Rock coast erosion: An overlooked source of sediments to the ocean. Europe as an example. Earth Planet. Sci. Lett. 579, 117356. https://doi.org/10.1016/j.epsl.2021.117356

Ricci, J., Lahitte, P., Quidelleur, X., 2015a. Construction and destruction rates of volcanoes within tropical environment: Examples from the Basse-Terre Island (Guadeloupe, Lesser Antilles). Geomorphology 228, 597–607. https://doi.org/10.1016/j.geomorph.2014.10.002

Ricci, J., Quidelleur, X., Lahitte, P., 2015b. Volcanic evolution of central Basse-Terre Island revisited on the basis of new geochronology and geomorphology data. Bull. Volcanol. 77, 1–17.

Robert, S., 2019. L'urbanisation du littoral : espaces, paysages et représentations. Des territoires à l'interface ville-mer (Habilitation à diriger des recherches). Université de Bretagne Occidentale (UBO), Brest.

Rohling, E.J., Grant, K., Bolshaw, M., Roberts, A.P., Siddall, M., Hemleben, C., Kucera, M., 2009. Antarctic temperature and global sea level closely coupled over the past five glacial cycles. Nat. Geosci. 2, 500–504.

Rohmer, J., Dewez, T., 2013. On the deviation of extreme sea-cliff instabilities from the power-law frequency-volume distribution: practical implications for coastal management. J. Coast. Res. 1698–1703.

Rosser, N.J., Brain, M.J., Petley, D.N., Lim, M., Norman, E.C., 2013. Coastline retreat via progressive failure of rocky coastal cliffs. Geology 41, 939–942.

Roulland, T., Maquaire, O., Costa, S., Compain, V., Davidson, R., Medjkane, M., 2019. Dynamique des falaises des Vaches Noires: analyse diachronique historique et récente à l'aide de documents multi-sources (Normandie, France). Géomorphologie Relief Process. Environ. 25, 37–55.

Rusu, L., Guedes Soares, C., 2012. Wave energy assessments in the Azores islands. Renew. Energy 45, 183–196. https://doi.org/10.1016/j.renene.2012.02.027

Salvany, T., Lahitte, P., Nativel, P., Gillot, P.-Y., 2012. Geomorphic evolution of the Piton des Neiges volcano (Réunion Island, Indian Ocean): competition between volcanic construction and erosion since 1.4 Ma. Geomorphology 136, 132–147.

Shackleton, N.J., 2000. The 100,000-year ice-age cycle identified and found to lag temperature, carbon dioxide, and orbital eccentricity. Science 289, 1897–1902.

725 Shepard, F.P., 1973. Submarine Geology. 3d edi-tion. Harper & Row, New York. 517pp.

Sherrod, D.R., Hagstrum, J.T., McGeehin, J.P., Champion, D.E., Trusdell, F.A., 2006. Distribution, 14C chronology, and paleomagnetism of latest Pleistocene and Holocene lava flows at Haleakalā volcano, Island of Maui, Hawai'i: A revision of lava flow hazard zones. J. Geophys. Res. Solid Earth 111. https://doi.org/10.1029/2005JB003876

Spratt, R.M., Lisiecki, L.E., 2016. A Late Pleistocene sea level stack. Clim. Past 12, 1079–1092.

730 Sunamura, T., 1992. Geomorphology of rocky coasts. Wiley.

Torrecillas, C., Berrocoso, M., Felpeto, A., Torrecillas, M.D., Garcia, A., 2013. Reconstructing palaeo-volcanic geometries using a Geodynamic Regression Model (GRM): Application to Deception Island volcano (South Shetland Islands, Antarctica). Geomorphology 182, 79–88. https://doi.org/10.1016/j.geomorph.2012.10.032

Trenhaile, A.S., 2001. Modelling the Quaternary evolution of shore platforms and erosional continental shelves. Earth Surf.
735 Process. Landf. J. Br. Geomorphol. Res. Group 26, 1103–1128.

Trenhaile, A.S., 2000. Modeling the development of wave-cut shore platforms. Mar. Geol. 166, 163–178.

Trenhaile, A.S., 1972. The Shore Platforms of the Vale of Glamorgan, Wales. Trans. Inst. Br. Geogr. 127–144. https://doi.org/10.2307/621545

Trenhaile, A.S., Bryne, M.-L., 1986. A Theoretical Investigation of the Holocene Development of Rock Coasts, with
740 Particular Reference to Shore Platforms. Geogr. Ann. Ser. Phys. Geogr. 68, 1–14. https://doi.org/10.1080/04353676.1986.11880154

Waelbroeck, C., Labeyrie, L., Michel, E., Duplessy, J.-C., Mcmanus, J.F., Lambeck, K., Balbon, E., Labracherie, M., 2002. Sea-level and deep water temperature changes derived from benthic foraminifera isotopic records. Quat. Sci. Rev. 21, 295–305.

745 Wright, L.W., 1970. Variation in the level of the cliff/shore platform junction along the south coast of Great Britain. Mar. Geol. 9, 347–353. https://doi.org/10.1016/0025-3227(70)90023-X

Ye, F.-Y., Barriot, J.-P., Carretier, S., 2013. Initiation and recession of the fluvial knickpoints of the Island of Tahiti (French Polynesia). Geomorphology 186, 162–173. https://doi.org/10.1016/j.geomorph.2012.12.031

Young, A.P., 2018. Decadal-scale coastal cliff retreat in southern and central California. Geomorphology 300, 164–175.

750 Young, A.P., Carilli, J.E., 2019. Global distribution of coastal cliffs. Earth Surf. Process. Landf. 44, 1309–1316.

Young, A.P., Guza, R.T., Matsumoto, H., Merrifield, M.A., O'Reilly, W.C., Swirad, Z.M., 2021. Three years of weekly observations of coastal cliff erosion by waves and rainfall. Geomorphology 375, 107545.